Teagle, D.A.H., Wilson, D.S., Acton, G.D., and Vanko, D.A. (Eds.)
Proceedings of the Ocean Drilling Program, Scientific Results Volume 206

2. Upper Cenozoic Calcareous Nannofossil Biostratigraphy and Inferred Sedimentation, ODP Leg 206, East Pacific Rise[1]

Shijun Jiang[2] and Sherwood W. Wise, Jr.[2]

ABSTRACT

Site 1256 of Ocean Drilling Program Leg 206 to the Guatemala Basin on the eastern flank of the East Pacific Rise yielded a near-complete, middle Miocene–Quaternary carbonate-rich section that provides an opportunity to study low-latitude biostratigraphic and paleoceanographic events. The sedimentary sequence in Hole 1256B has been zoned using calcareous nannofossils according to the biostratigraphic schemes by Martini of 1971 (modified by Martini and Müller in 1986) and Okada and Bukry of 1980. The nannofossil assemblage is characteristic of the low latitudes, with abundant *Gephyrocapsa, Discoaster,* and *Sphenolithus,* and is in general moderately to well preserved, depending on nannofossil abundance and the presence of diatoms. Age estimates for the first occurrence and last occurrence of *Reticulofenestra rotaria* were derived from biostratigraphy and magnetostratigraphy independently and assigned to 7.18 and 6.32 Ma, respectively.

Linear sedimentation rates, calculated using 28 nannofossil datums and age estimates, are high in the middle Miocene, decrease from the late Miocene to the Pliocene, then increase upsection. The abrupt drop in carbonate mass accumulation rates during the early late Miocene is referred to as the "carbonate crash." This pattern reflects (1) the long-trend decrease of productivity as the site moves away from the upwelling system at the equatorial divergence as well as (2) fluctuation in the chemistry of the bottom waters associated with production of the North Atlantic Bottom Water and ventilation via the Panama Gateway.

[1]Jiang, S., and Wise, S.W., Jr., 2007. Upper Cenozoic calcareous nannofossil biostratigraphy and inferred sedimentation, ODP Leg 206, East Pacific Rise. *In* Teagle, D.A.H., Wilson, D.S., Acton, G.D., and Vanko, D.A. (Eds.), *Proc. ODP, Sci. Results,* 206: College Station, TX (Ocean Drilling Program), 1–25. doi:10.2973/odp.proc.sr.206.008.2007
[2]Department of Geological Sciences, Florida State University, Tallahassee FL 32306-4100, USA. Correspondence author: **jiang@gly.fsu.edu**

Initial receipt: 2 May 2005
Acceptance: 17 April 2006
Web publication: 9 January 2007
Ms 206SR-008

A basement age of 14.5 Ma was obtained by extrapolating the 39.1-m/m.y. rate in the middle Miocene to the basement at 250.7 meters below seafloor, and is consistent with the ~15-Ma age of the oceanic crust estimated from marine magnetic anomalies. Reworked nannofossils and lithologic changes were used to unravel postdepositional history, and three episodes were recognized, one of which in the latest Miocene can be widely correlated.

INTRODUCTION

Ocean Drilling Program (ODP) Leg 206 is the first of a multileg campaign to sample a complete crustal section from the extrusive lavas, through the sheeted dike complex, and into the uppermost gabbros within in situ ocean crust, by drilling a deep hole into basement formed at a superfast spreading rate (Shipboard Scientific Party, 2003). Site 1256 (6°44.2′N, 91°56.1′W; Fig. **F1**) lies in 3635 m of water in the Guatemala Basin on Cocos plate crust that formed ~15 m.y. ago on the eastern flank of the East Pacific Rise (EPR) when the site experienced superfast spreading (Wilson, 1996). This site formed at an equatorial latitude (Fig. **F1**) within the equatorial high-productivity zone and initially endured very high sedimentation rates (>35 m/m.y.) (e.g., Shipboard Scientific Party, 2003).

Three holes were drilled at Site 1256 with the intention of retrieving sediments. Hole 1256A produced a single mudline core that recovered the uppermost 2.37 m of the sedimentary section. This interval was resampled using the advanced piston corer (APC) with a second mudline core in Hole 1256B, where coring continued to a depth of 250.70 meters below seafloor (mbsf), at which point basement was contacted. Roughly 1 m more penetration recovered ~5 cm of the uppermost basalt. The lower portion of the sedimentary section was resampled in the rotary-cored Hole 1256C from a depth of 220.10 to 245 mbsf. Sediments in Hole 1256B provide a complete sampling of the sedimentary sequence overlying the oceanic basement. The sediments are subdivided into two principal lithologic units. Unit I (0–40.6 mbsf) is clay rich with a few carbonate-rich intervals and becomes increasingly calcareous with depth. Unit II (40.6–250.7 mbsf) is predominantly biogenic carbonate with some minor more siliceous and diatom-rich intervals. Bioturbation is common throughout the whole sedimentary sequence.

Calcareous nannofossils are generally abundant and moderately to well preserved in all samples from Site 1256. Preservation and individual nannofossil species abundance are recorded in Table **T1.** All species considered in this report are listed in alphabetical order in the distribution chart (Table **T1**) and the **"Appendix,"** p. 17. Descriptions of species and genera noted in this study and their bibliographic references are given in Perch-Nielsen (1985), Bown (1998), and Wise et al. (2004).

This chapter examines the nannofossil biostratigraphy of Hole 1256B and some associated postdepositional events from the middle Miocene to the Quaternary. The biostratigraphy for the sedimentary sequence immediately above the crust provides a useful tool for dating the underlying oceanic crust because direct dating of usually altered oceanic basalts has seldom been possible. Correlation of nannofossil datums in eastern equatorial Pacific (EEP) drill holes would indicate intra- and interplate variations in geologic and tectonic history.

F1. Backtracked path for Leg 206 Site 1256, p. 20.

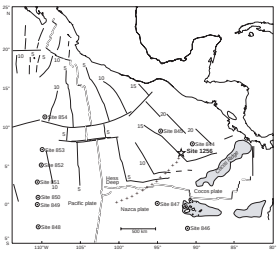

T1. Calcareous nannofossil distribution chart in Hole 1256B, p. 24.

MATERIALS AND METHODS

A total of 291 samples were taken aboard *JOIDES Resolution* at 2 per section (at a sample spacing of 75 cm) for all cores from Hole 1256B, and smear slides were made for all samples. Preparation of smear slides followed standard techniques using Norland-61 optical adhesive as a mounting medium. Slides were examined using a Zeiss Axioskop II microscope under cross-polarized light, transmitted light, and phase-contrast light at 800× and 1250× magnification. A JEOL JSM 840 scanning electron microscope (SEM) was employed to take digital images for more precise species identification. Relative abundance of individual nannofossil species and overall preservation and abundance of the nannofossil assemblages were recorded in semiquantitative estimates under a magnification of 1000× for each sample. Letter codes for these estimates follow those of Arney and Wise (2003) as below.

Estimates of overall nannofossil abundance were given the following letter codes:

V = very abundant (>10 nannofossils per field of view).
A = abundant (1–10 nannofossils per field of view).
C = common (1 nannofossil per 2–10 fields of view).
F = few (1 nannofossil per >10–100 fields of view).
R = rare (1 nannofossil per >100 fields of view).
B = barren (no nannofossils per >500 fields of view).

The average state of preservation of the nannofossil assemblage in each sample is designated as follows with transitional conditions between them:

VG = very good (no evidence of dissolution and/or overgrowth; no alteration of primary morphological characteristics and specimens appear diaphanous; specimens are identifiable to the species level).
G = good (little or no evidence of dissolution and/or overgrowth; primary morphological characteristics only slightly altered; specimens are identifiable to the species level).
M = moderate (specimens exhibit some etching and/or overgrowth; primary morphological characteristics sometimes altered; however, most specimens are identifiable to the species level).
P = poor (specimens are severely etched or exhibit overgrowth; primary morphological characteristics largely destroyed; fragmentation has occurred; specimens cannot be identified at the species and/or generic level).

Relative individual species abundance estimations follow the procedure of Hay (1970) as below:

V = very abundant (>10–100 specimens per field of view).
A = abundant (1–10 specimens per field of view).
C = common (1 specimen per 2–10 fields of view).
F = few (1 specimen per 11–100 fields of view).
R = rare (1 specimen per 101–1000 fields of view).

BIOSTRATIGRAPHY RESULTS

The nannofossil zonation schemes proposed by Martini (1971; modified in Martini and Müller, 1986) and Okada and Bukry (1980) for low latitudes were used as the basic zonal reference in this study. Absolute ages were assigned to all datum levels to facilitate derivation of sedimentation rates and easy comparison with other studies. Most ages were compiled from Berggren et al. (1995a, 1995b), and a few were compiled from other commonly cited sources (Table T2). The positions of biostratigraphic datums and their numerical ages are presented in Table T2.

T2. Age estimate, depth, and zonation of calcareous nannofossils, p. 25.

Quaternary (0–1.77 Ma)

The calcareous nannofossils recovered from the Quaternary are generally abundant to common and moderately preserved in Hole 1256B and have been affected to different degrees mainly by etching and fragmentation. No significant reworking of nannofossils was apparent, and the sparse occurrence of reworked discoasterids and sphenoliths in a few samples did not hinder the recognition of zonal datums. The assemblages have low diversity, with ~17–21 species, and are characterized by abundant to common *Gephyrocapsa, Reticulofenestrata, Calcidiscus,* and zonal markers for the specific zones.

Zone NN21 (CN15; 0–0.26 Ma)

Sediments downhole to Sample 206-1256B-1H-2, 40–42 cm (1.90 mbsf), were placed in this zone. The base of this zone is defined by the first occurrence (FO) of *Emiliania huxleyi,* for which recognition required confirmation under SEM due to its tiny size (2–4 µm).

Zone NN20 (CN14b; 0.26–0.46 Ma)

Samples 206-1256B-1H-3, 40–42 cm (3.40 mbsf), and 1H-4, 40–42 cm (4.90 mbsf), were assigned to Zone NN20, which is a "gap" zone defined by the presence of *Gephyrocapsa* and absence of *E. huxleyi* and *Pseudoemiliania lacunosa*. The barren Sample 206-1256B-1H-3, 115–117 cm (2.65 mbsf), immediately overlying this interval renders the NN21/NN20 boundary uncertain.

Zone NN19 (CN14a–CN13; 0.46–1.95 Ma)

This interval lies between the last occurrences (LOs) of *P. lacunosa* in Sample 206-1256B-1H-4, 115–117 cm (5.65 mbsf), and the apparent LO of *Discoaster brouweri* in Sample 3H-3, 115–117 cm (19.75 mbsf). Another three datums, the LO of *Helicosphaera sellii,* LO of *Calcidiscus macintyrei,* and FO of *Gephyrocapsa caribbeanica,* which are present in Samples 206-1256B-2H-CC (15.91 mbsf), 3H-1, 115–117 cm (16.75 mbsf), and 3H-1, 40–42 cm (16.00 mbsf), respectively, can be used to refine this interval according to Gartner (1977), Okada and Bukry (1980), and Raffi et al. (1993). Their ages are listed in Table T2 but not described in detail here.

Pleistocene/Pliocene Boundary

The transition from the Pliocene to Pleistocene at Site 1256 is marked by an interval barren of nannofossils that spans from Samples 206-1256B-3H-2, 40–42 cm (17.50 mbsf), to 3H-3, 40–42 cm (19.00 mbsf), and falls within Zones NN19 and NN18. The Pleistocene/Pliocene boundary is arbitrarily placed at the top of this interval (17.50 mbsf), which closely approximates the lithologic Subunit IA/IB boundary at a sediment color change at Section 206-1256B-3H-2, 38 cm (17.48 mbsf). This boundary, with an age of 1.78 Ma (Berggren et al., 1995b), is above the apparent LO of *D. brouweri* (1.95 Ma) in Sample 206-1256B-3H-3, 40–42 cm (19.75 mbsf).

Pliocene (1.77–5.32 Ma)

Nannofossils recorded from the Pliocene generally have a higher abundance relative to the Quaternary, except that there are several intervals barren of nannofossils and the abundance increases with depth. The preservation of nannofossil assemblages ameliorates with increasing depth and is closely associated with the presence and abundance of diatoms, which release silica to pore waters and thus inhibit dissolution and/or precipitation of calcite during diagenesis (Wise, 1977). The assemblages above Zone NN15 remain low in diversity and contain abundant to common reticulofenestrids, discoasterids, coccoliths, and *Calcidiscus*. Downhole from Zone NN15, the diversity and abundance of nannofossils increases abruptly, which is caused by the dominance and diversification of reticulofenestrids and sphenoliths.

Zone NN18 (CN12d; 1.95–2.44 Ma)

Samples 206-1256B-3H-3, 115–117 cm (19.75 mbsf), to 3H-5, 115–117 cm (22.75 mbsf), are assigned to Zone NN18. The interval is normally defined as the LO of *Discoaster pentaradiatus* to the LO of *D. brouweri*. Assuming a normal stratigraphic order by stratigraphic sequence, the nannofossil-barren intervals at the top and bottom of this zone can be constrained by the overlying and underlying biozones and are assigned to the combined Zones NN19–NN18 and NN18–NN17, respectively; hence, the upper and lower boundaries of Zone NN18 are uncertain. The apparent LO of *Ceratolithus rugosus* is also recorded in the same sample as *D. brouweri* (Sample 206-1256B-3H-3, 115–117 cm [19.75 mbsf]).

Zone NN17 (CN12c; 2.44–2.61 Ma)

As mentioned above, the upper boundary of this zone lies in a nannofossil-barren interval and thus remains uncertain. The base of this zone is recorded above Sample 206-1256B-4H-2, 40–42 cm (27.00 mbsf), based on the LO of *Discoaster surculus* in this sample.

Zone NN16 (CN12a–CN12b; 2.61–3.75 Ma)

This zone is assigned to Samples 206-1256B-4H-2, 40–42 cm (27.00 mbsf), through 4H-4, 40–42 cm (30.00 mbsf), based on the LO of *Reticulofenestra pseudoumbilica* in the underlying Sample 4H-4, 115–117 (30.75 mbsf), a species defined by a minimum coccolith length of >7 µm. An alternative zonal marker proposed by Okada and Bukry (1980)

for the base of this zone is the LO of *Sphenolithus abies/neoabies,* which occurs a little higher in stratigraphic position and was recorded in the lowermost sample of this zonal interval. The presence of a barren sample in the middle of this interval does not prohibit placement of the zonal boundaries.

Zone NN15 (CN11; 3.75–4.8 Ma)

This zone encompasses Samples 206-1256B-4H-4, 115–117 cm (30.75 mbsf), through 5H-1, 115–117 cm (35.75 mbsf), which directly overly the LO of *Amaurolithus primus* in Sample 5H-2, 40–42 cm (36.50 mbsf), an equivalent zonal marker proposed by Okada and Bukry (1980) to replace the rare *Amaurolithus tricorniculatus*. The latter only occurs in Sample 206-1256B-5H-2, 115–117 cm (37.25 mbsf).

Zone NN14–NN13 (CN10c; 4.8–5.04 Ma)

Sediments between Samples 206-1256B-5H-2, 40–42 cm (36.50 mbsf), and 5H-3, 115–117 cm (38.75 mbsf), an interval directly above the LO of *C. rugosus* in Sample 5H-4, 40–42 cm (39.50 mbsf), are assigned to this combined zone. Another useful datum, the LO of *Ceratolithus acutus,* occurs in Sample 206-1256B-5H-2, 115–117 cm (37.25 mbsf). No attempt was made to determine the FO of *Discoaster asymmetricus,* a datum defining the boundary between Zones NN14 and NN13, because of the intermittent occurrence of this species.

Zone NN12 (CN10a–CN10b; 5.04–5.34 Ma)

This zone is recorded in the interval from Samples 206-1256B-5H-4, 40–42 cm (39.50 mbsf), to 5H-5, 115–117 cm (41.75 mbsf), where both *C. rugosus* and *Discoaster quinqueramus* are absent. The FO of *C. acutus* falls within this zone, which helps in the recognition of this "gap" zone.

Pliocene/Miocene Boundary

The Pliocene/Miocene boundary in terms of calcareous nannofossils falls within Subzone CN10a or Zone NN12 (Perch-Nielsen, 1985). The FO of *C. acutus* closely approximates this epoch boundary, which lies just above the extinction of *D. quinqueramus,* a well-documented datum level in most sections.

Miocene (5.32–23.80 Ma)

Nearly all the Miocene samples examined contain very abundant and diversified nannofossil assemblages. These assemblages are generally moderately to well preserved but deteriorate downhole, due mainly to overgrowth as well as dissolution. Similar to preservation in the overlying Pliocene assemblages, the preservation depends to a great extent on the presence and abundance of diatoms. The assemblages consist of highly diversified and predominant reticulofenestrids, discoasterids, sphenoliths, coccoliths, and *Calcidiscus*.

Zone NN11 (CN9; 5.6–8.6 Ma)

This zone covers the stratigraphic range of *D. quinqueramus,* which was observed between Samples 206-1256B-5H-6, 40–42 cm (42.50 mbsf), and 9H-6, 40–42 cm (80.50 mbsf); in the latter sample, the FO of *Discoaster berggrenii* was documented. The FO of *A. primus,* located in Sample 206-1256B-7H-7, 40–42 cm (63.00 mbsf), is used to subdivide this thick zone into upper Subzone NN11b and lower Subzone NN11a. Two other events, the LO and FO of *Amaurolithus amplificus* in Samples 206-1256B-6H-3, 40–42 cm (47.50 mbsf), and 7H-3, 40–42 cm (57.00 mbsf), respectively, can be used with caution because of its generally rare occurrence to further refine Subzone NN11b.

The LO and FO of *Reticulofenestra rotaria,* a circular placolith with a relatively large central opening and a diameter of 5–7 µm, recorded in Samples 206-1256B-6H-6, 115–117 cm (52.75 mbsf), through 7H-CC (63.39 mbsf), between Chrons C3An.2n (t) (51.60 mbsf) and C4n.1n (o) (71.56 mbsf) (Shipboard Scientific Party, 2003), have the stratigraphic potential to refine Subzone NN11b. Assuming a constant sedimentation rate, derived independently from biostratigraphy and magnetostratigraphy, the FO is calculated at 7.18 and 7.03 Ma and the LO is calculated at 6.32 and 6.34 Ma, respectively. The difference in the age estimates probably arises from sedimentation rate variation and sample spacing for biostratigraphy; the latter issue in sample spacing could be resolved by further closer sampling. Considering the stratigraphic distribution of *R. rotaria, A. primus,* and *A. amplificus* in the sequence (Table **T1**), the ages for the FO and LO of *R. rotaria* are assigned to 7.18 and 6.32 Ma, respectively. Taking into consideration the differences in timescales used in both studies, these assignments are reasonably consistent with those calibrated by Wei (1995).

Zone NN10 (CN8; 8.6–9.4 Ma)

This zone is assigned to Samples 206-1256B-9H-6, 115–117 cm (81.25 mbsf), through 10H-2, 40–42 cm (84.00 mbsf), the base of which is defined by the LO of *Discoaster hamatus* in Sample 10H-2, 115–117 cm (84.75 mbsf). This datum coincides with the LO of *Discoaster bollii* in this hole. The presence of *Discoaster neorectus* aids in identifying this gap zone.

Zone NN9 (CN7; 9.4–10.38 Ma)

This zone spans the stratigraphic range of *D. hamatus* and encompasses Samples 206-1256B-10H-2, 115–117 cm (84.75 mbsf), through 12H-2, 115–117 cm (103.75 mbsf). Shipboard observation of this marker in Sample 206-1256B-10H-4, 100 cm (87.60 mbsf), is consistent with this assignment. Because the upper boundary is populated by the rare and sparse occurrence of this species and there exist samples bearing very few or no nannofossils, the precise placement requires much effort. It is worth mentioning that the occurrences of this zonal marker in Samples 206-1256B-9H-4, 40–42 cm (77.50 mbsf), and 9H-4, 115–117 cm (78.25 mbsf), are considered to be reworked, the significance of which will be discussed in **"Discussion,"** p. 8. The LO of *Catinaster coalitus* recorded in Sample 206-1256B-11H-3, 115–117 cm (95.75 mbsf), can be used to subdivide this zone. The intermittent occurrence of *Discoaster neohamatus* in the lower part of its range at this site renders the application of its FO datum impossible.

Zone NN8 (CN6; 10.38–10.9 Ma)

This zone lies between the FOs of *D. hamatus* and *C. coalitus,* the latter datum being observed in Sample 206-1256B-12H-4, 40–42 cm (106.00 mbsf). The LO of *Coccolithus miopelagicus* approximates the top of this zone.

Zone NN7 (CN5b; 10.9–11.8 Ma)

Zone NN7 is recorded by the FO of *C. coalitus* downhole to the FO of *Discoaster kugleri* in Sample 206-1256B-17H-1, 40–42 cm (149.00 mbsf). The preservation of nannofossils deteriorates with depth from the middle of this zone, which makes differentiation among discoaster species difficult. *D. kugleri,* however, can still be distinguished from *Discoaster sanmiguelensis* and other discoasterids in overgrown specimens by the diagnostic six short rays and a broad, flat central area. Its LO recorded in Sample 206-1256B-14H-CC (130.05 mbsf), provides a datum to further subdivide this thick interval.

Zone NN6 (CN5a; 11.8–13.6 Ma)

The lowermost biostratigraphic zonal event in the section, the LO of *Sphenolithus heteromorphus,* the specimens of which are overgrown but recognizable by their diagnostic bright apical spines and butterfly-shaped bases, marks the base of Zone NN6 in Sample 206-1256B-25X-1, 115–117 cm (214.15 mbsf). Here *Cyclicargolithus floridanus,* the last continuous occurrence of which is in Sample 206-1256B-23X-CC (202.77 mbsf), provides a further datum to subdivide Zone NN6. This additional datum provides a sound biostratigraphic correlation line in equatorial areas (Raffi et al., 1995).

Zone NN5 (CN4; 13.6–15.6 Ma)

Helicosphaera ampliaperta, the LO of which marks the base of Zone NN5, was absent from all samples including the lowermost Sample 206-1256B-28X-CC (245.83 mbsf). This indicates that the basaltic basement underlying the sedimentary sequence is younger than 15.6 Ma (age of the LO of *H. ampliaperta*). The rare and sparse, but distinctive, onset of *R. pseudoumbilica* is in Sample 206-1256B-26X-3, 40–42 cm (226.10 mbsf), and provides a useful datum to assess the age of basement. Assuming a constant sedimentation rate of 39.1 m/m.y., based on datums from below 100 mbsf, a basement age of ~14.5 Ma is implied (Fig. F2), consistent with the assignment to Zone NN5 of the middle Miocene. This age is reasonably consistent with the age of 15.1 Ma inferred from magnetic anomalies (Shipboard Scientific Party, 2003).

F2. Linear sedimentation rates and age-depth plots, p. 21.

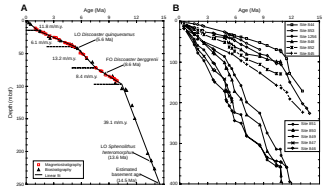

DISCUSSION

With two-thirds of the cores taken by APC as well as good sediment recovery via rotary coring, Leg 206 has added considerably to the sediment recovery for this region. The high core recovery (89%) provides an excellent opportunity to study environmental, oceanographic, and biotic changes from the middle Miocene to the Holocene in the equatorial Pacific. Sedimentation rates especially were generally high in those critical time intervals, which is ideal for high-resolution biostratigraphic and paleoceanographic studies.

Sedimentation History

Linear sedimentation rates, uncorrected for compaction, were calculated based on 28 nannofossil age estimates in Table T2 for the sedimentary sequence of Hole 1256B and plotted with best-fit lines. Sedimentation rates vary from 6.1 to 39.1 m/m.y. (Fig. F2A). Calculated sedimentation rates are high in the middle Miocene (39.1 m/m.y.), decrease drastically in the lower upper Miocene (8.4 m/m.y.), recover somewhat in the uppermost Miocene (13.2 m/m.y.), and reach the lowest point in the Pliocene (6.1 m/m.y.), but they increase thereafter (11.8 m/m.y.).

In order to illustrate changes in depositional environments and processes through time at Site 1256, mass accumulation rates (MARs) have been calculated for bulk sediments and the main sedimentary components such as calcium carbonate, terrigenous material, and biogenic silica (Fig. F3).

Calcium carbonate MARs show an abrupt transition at ~11 Ma, which coincides with a "diatom mat" (i.e., a series of diatom-rich laminae that occur at this horizon throughout the region; see Kemp and Baldauf, 1993). Carbonate MARs are high except for a major drop at ~12.9 Ma during the middle Miocene, remain extremely low from ~10.2 to 9.1 Ma, recover somewhat from 9 to ~5 Ma, and stay particularly low thereafter.

This pattern of variations in sedimentation was also observed at Sites 844–853 drilled during ODP Leg 138 (Fig. F1). Although there is a difference in proximity to continents and in water depths among sites located in Guatemala Basin (Sites 844, 845, and 1256), sedimentation rates positively covary (Fig. F2B), and sedimentary thickness during a specific time interval shows little variation (Fig. F4). This suggests that these sites have experienced a virtually same sedimentation history and terrestrial influences have remained a minor factor from the middle Miocene through the Quaternary. This, together with the fact that positions of the epoch boundaries are closely related to water depths (Fig. F4), reflects virtually no intraplate variation in geological and tectonic settings on Cocos plate.

The nature of deposition in EEP has been influenced mainly by surface water productivity. Sites on the Cocos and Nazca plates are separated from the west coast of Central America by the Middle America Trench, which traps most terrestrial sediments shed from the continent, and sites on the Pacific plate are far removed from continents. The sedimentary sources, therefore, are mainly biogenic calcite and silica, which determine the sedimentation rates (e.g., at Site 1256 [Fig. F3]). This is further confirmed by the close correlation between $CaCO_3$ MARs and Ba/Ti ratios, chemical proxies for biogenic productivity (Shipboard Scientific Party, 2003).

The distribution pattern of surface water productivity today helps explain the spatial and temporal variations in EEP. The V-shape profile in the longitudinal transect along Sites 848–853 clearly reflects diminishing productivity away from the Equator (Fig. F4), as seen today (Paytan et al., 1996). Sites with substantially higher sedimentation rates are located under highly productive waters (e.g., Sites 849–851 under the equatorial divergence and Sites 846–847 close to the Galápagos Islands under strong influence of the Peru upwelling system). These sites have been remaining under this situation since middle Miocene because of a moving path nearly parallel to the Equator (Pisias et al., 1995). The high biological productivity fuels the high sedimentation

F3. Relationship of MARs, p. 22.

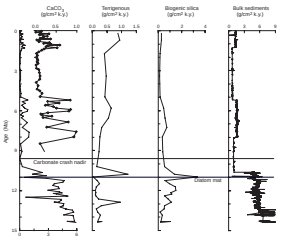

F4. Correlation of nannofossil datums in EEP drill holes, p. 23.

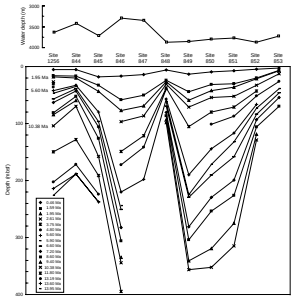

rates. Conversely, the diminishing productivity has resulted in a decrease in sedimentation rates as sites on the Cocos plate (Sites 844, 845, and 1256) move away from the Equator.

The high sedimentation rates in the middle Miocene can be attributed to high productivity and good preservation while these sites were near the paleoequator on young, shallow seafloor. This is indicated by a nannofossil assemblage showing little dissolution at Site 1256. The lowest sedimentation rates (Pliocene), however, likely have resulted from intense dissolution superimposed on reduced paleoproductivity as indicated by the poor to moderate preservation of nannofossils and nannofossil-barren intervals at Site 1256. This probably resulted from a combination of seafloor subsidence and a shoaling of the calcite compensation depth (CCD) associated with a change in chemistry of deep waters and/or surface carbonate production.

Carbonate Crash

The major middle–late Miocene carbonate shift recorded at Site 1256 is referred to as the carbonate crash by Lyle et al. (1995) and Farrell et al. (1995). This event has been widely recorded in the Pacific and Atlantic Oceans and Caribbean Sea (Berger, 1970; King et al., 1997; Roth et al., 2000) and provides a seismic reflector for long-range correlation (Mayer et al., 1986; Bloomer et al., 1995). Lyle et al. (1995) and Farrell et al. (1995) attributed the carbonate crash to enhanced dissolution associated with changes in bottom water characteristics, rather than with changes in productivity. Emerson and Bender (1981) and Archer (1991a, 1991b), however, have demonstrated that under proper conditions, increases in productivity can lead to enhanced dissolution through acids produced by the degradation of organic matter. Lyle et al. (1995) cited a decrease rather than increase of organic carbon to support their argument, which seems plausible because such a decrease in organic carbon can also be caused by enhanced degradation resulting in higher acid production. In such a case, the organic carbon cannot be used as a proxy of productivity.

Several mechanisms have been proposed for the carbonate crash. Even though there is an apparent correlation of the carbonate crash and a eustatic sea level drop (Haq et al., 1987), Peterson et al. (1992) showed that globally, the middle–late Miocene sea level drop is associated with deepening of the CCD and enhanced carbonate preservation. This is supported by Berger's (1970) basin-shelf fractionation model. Other causative mechanisms proposed, such as the constriction of the Panama Gateway (Lyle et al., 1995) and the initiation of North Atlantic Deep Water (NADW) (Woodruff and Savin, 1989), account for the crash by enhanced corrosiveness of bottom water imported into this region.

The arguments presented above clearly show that the middle–late Miocene carbonate crash is still not resolved in terms of the interplay of dissolution and production. Dissolution seems to play a certain role associated with large variations in the CCD, with nearly complete carbonate dissolution during brief intervals when the CCD shoaled by as much as 1400 m (van Andel et al., 1975). However, the cause of enhanced dissolution is complex but probably relates to (1) tectonic movement associated with the Panama Gateway and a slowdown of seafloor spreading, as indicated by the magnetic anomaly pattern in Figure **F1;** and (2) phytoplankton productivity associated with ocean circulation patterns.

Evidence from calcareous nannofossils and diatoms tends to attribute it to surface water process. Prior to the carbonate crash, all major reductions in carbonate resulted from deposition of laminated diatom oozes (Kemp, 1995), which is believed to be controlled by surface process, instead of dissolution at depth (Kemp et al., 1995). At Site 1256, the calcareous nannofossil assemblages exhibit their best preservation just prior to the carbonate crash nadir. The same is true at Site 846 (Raffi and Flores, 1995). This proposal is consistent with the study in terms of stable isotopes (**Jiang et al.,** this volume).

Downslope Transport of Sediments

Calcareous nannofossils are susceptible to reworking because of their tiny size; hence, reworked fossils often pose problems in biostratigraphy. Some of them with a short range but that are clearly out of place (e.g., *D. hamatus*), together with lithologic information, however, provide an opportunity to study episodes of redeposition. For example, downhole investigation of nannofossils found *D. quinqueramus* and *D. hamatus* together in Samples 206-1256B-9H-4, 40–42 cm (77.50 mbsf), and 9H-4, 115–117 cm (78.25 mbsf), which caused confusion in interpreting the biostratigraphy. Upon close examination of more samples, the isolated occurrences of *D. hamatus* in these two samples seem more likely to be reworked, and hence its actual LO should be much lower, which is supported by the sudden sedimentary color change. Based on the criteria of reworked fossils and abrupt lithologic change, three episodes of redeposition were recognized, and the timing for these were obtained from the age-depth plot assuming constant sedimentation rates for the specific interval:

Episode 1: This reworking episode is recognized at Section 206-1256B-5H-1, 108 cm (35.68 mbsf), which dates to ~4.7 Ma. It is recognized by the common reoccurrence of *D. berggrenii* and *D. quinqueramus* from Zone NN11 along with *Sphenolithus moriformis* in Samples 206-1256B-4H-CC (35.23 mbsf), and 5H-1, 40–42 cm (35.00 mbsf). Note the deeper depth of Sample 206-1256B-4H-CC, relative to 5H-1, 40–42 cm, because of the >100% core recovery for Core 4H. A sharp uphole change in sediment color from dark brown to gray brown and reduced bioturbation occur across the boundary.

Episode 2: Against the normal background deposition in Zone NN11, characterized by the presence of *D. quinqueramus* and *D. berggrenii,* reworked specimens of *D. hamatus* and *D. bollii* stand out in Samples 206-1256B-9H-4, 40–42 cm (77.50 mbsf), and 9H-4, 115–117 cm (78.25 mbsf). The conspicuous sudden reduction in bioturbation upward and sedimentary color change from green gray to dark green co-occurs right between Sections 206-1256B-9H-4 and 9H-5, and the boundary between these is placed at Section 9H-4, 150 cm (78.60 mbsf), with an age of ~8.3 Ma.

Episode 3: The oldest redepositional event is recognized at Section 206-1256B-11H-6, 95 cm (100.05 mbsf), and is dated at 10.7 Ma. It is signaled by reworked specimens of *C. abisectus* (Oligocene–early Miocene age) and an abrupt lithologic change. Upward across this boundary, there is not only a sudden change in sediment color from dark green gray to light green gray but also a loss of intense bioturbation.

These redepositional events provide cogent evidence for downslope processes active on the EPR throughout Neogene. It is worth noting that Episode 2 has been recorded in Knüttel's 1986 study on the EPR as well as in many ocean basins (Ciesielski and Wise, 1977; Adams et al., 1977). Knüttel (1986) suggested that a Messinian sea level drop triggered intensified bottom current activity, whereas Rea and Janecek (1986) alternatively interpreted this as tectonic instability associated with possible increased seismic activity. By either mechanism, however, turbidity currents have produced a rapid accumulation of sediments as indicated by the sharp sedimentary contacts and sharply reduced bioturbation.

CONCLUSIONS

The primary objective of this paper has been to refine middle Miocene–Quaternary nannofossil biostratigraphy of Site 1256 in the Guatemala Basin on Cocos plate crust and compare the data with those from other sites in this basin.

1. The middle Miocene–Quaternary sedimentary sequence at Site 1256 appears to be complete in terms of the calcareous nannofossil assemblage succession. A total of 16 zones/combined zones are recognized, and nearly all zonal boundaries are located within a quarter section of a core.
2. Age estimates for two nannofossil datums, 7.18 Ma for the FO and 6.32 Ma for the LO of *R. rotaria,* respectively, were derived from biostratigraphy and magnetostratigraphy.
3. Linear sedimentation rates were calculated using 28 nannofossil age estimates. Rates are high in the middle Miocene, decrease drastically in the lower upper Miocene, recover somewhat in the uppermost Miocene, and reach the lowest point in the Pliocene, but they increase thereafter. This pattern of variations is similar to that observed at nearby ODP sites in the Guatemala Basin. The middle–upper Miocene carbonate crash was observed. The crash is believed to have been caused by enhanced dissolution that resulted from lowered productivity as well as the initiation of NADW and the constriction of the Panama Gateway. These similar sedimentary patterns, together with the close correlation of epoch boundaries at Site 1256 to those published for other nearby Deep Sea Drilling Project/ODP sites, suggest virtually no intraplate variations on the Cocos plate in terms of depositional history.
4. Reworked nannofossils, together with sedimentation changes indicated by significant color change, were used to investigate redeposition events, and three episodes were recognized. The Messinian sea level drop and increased seismic activity may have contributed to intensified bottom current activity. Turbidity currents likely produced these episodes of redeposition as indicated by a sharp change in sediment color and a sharp reduction in bioturbation.

ACKNOWLEDGMENTS

We wish to thank all the participants of ODP Leg 206 for their contributions relevant to this paper and the members from the Calcareous

Nannofossil Laboratory at Florida State University for their helpful comments and assistance. We thank Drs. Gary Acton, José-Abel Flores, and Koji Kameo for helpful and constructive reviews. This research used samples and/or data provided by the Ocean Drilling Program (ODP). ODP is sponsored by the U.S. National Science Foundation (NSF) and participating countries under management of Joint Oceanographic Institutions (JOI), Inc. Funding for this research was provided by a United States Science Advisory Committee (USSAC) grant (Task Order F001790) to both authors.

REFERENCES

Adams, C.G., Benson, R.H., Kidd, R.B., Ryan, W.B.F., and Wright, R.C., 1977. The Messinian salinity crisis and evidence of late Miocene eustatic changes in the world ocean. *Nature (London, U. K.),* 269:383–386. **doi:10.1038/269383a0**

Archer, D., 1991a. Equatorial Pacific calcite preservation cycles: production or dissolution? *Paleoceanography,* 6(5):561–571.

Archer, D., 1991b. Modeling the calcite lysocline. *J. Geophys. Res.,* 96(C2):17037–17050.

Arney, J.E., and Wise, S.W., Jr., 2003. Paleocene–Eocene nannofossil biostratigraphy of ODP Leg 183, Kerguelen Plateau. *In* Frey, F.A., Coffin, M.F., Wallace, P.J., and Quilty, P.G. (Eds.), *Proc. ODP, Sci. Results,* 183: College Station, TX (Ocean Drilling Program). **doi:10.2973/odp.proc.sr.183.014.2003**

Backman, J., and Raffi, I., 1997. Calibration of Miocene nannofossil events to orbitally tuned cyclostratigraphies from Ceara Rise. *In* Shackleton, N.J., Curry, W.B., Richter, C., and Bralower, T.J. (Eds.), *Proc. ODP, Sci. Results,* 154: College Station, TX (Ocean Drilling Program), 83–99. **doi:10.2973/odp.proc.sr.154.101.1997**

Berger, W.H., 1970. Biogenous deep-sea sediments: fractionation by deep-sea circulation. *Geol. Soc. Am. Bull.,* 81:1385–1401.

Berggren, W.A., Hilgen, F.J., Langereis, C.G., Kent, D.V., Obradovich, J.D., Raffi, I., Raymo, M.E., and Shackleton, N.J., 1995a. Late Neogene chronology: new perspectives in high-resolution stratigraphy. *Geol. Soc. Am. Bull.,* 107:1272–1287. **doi:10.1130/0016-7606(1995)107<1272:LNCNPI>2.3.CO;2**

Berggren, W.A., Kent, D.V., Swisher, C.C., III, and Aubry, M.-P., 1995b. A revised Cenozoic geochronology and chronostratigraphy. *In* Berggren, W.A., Kent, D.V., Aubry, M.-P., and Hardenbol, J. (Eds.), *Geochronology, Time Scales and Global Stratigraphic Correlation*. Spec. Publ.—SEPM (Soc. Sediment. Geol.), 54:129–212.

Bloomer, S.F., Mayer, L.A., and Moore, T.C., Jr., 1995. Seismic stratigraphy of the eastern equatorial Pacific Ocean: paleoceanographic implications. *In* Pisias, N.G., Mayer, L.A., Janecek, T.R., Palmer-Julson, A., and van Andel, T.H. (Eds.), *Proc. ODP, Sci. Results,* 138: College Station, TX (Ocean Drilling Program), 537–553.

Bown, P.R. (Ed.), 1998. *Calcareous Nannofossil Biostratigraphy:* Dordrecht, The Netherlands (Kluwer Academic Publ.).

Ciesielski, P.F., and Wise, S.W., 1977. Geologic history of the Maruice Ewing Bank of the Falkland Plateau (southwest Atlantic sector of the Southern Ocean) based on piston and drill cores. *Mar. Geol.,* 25(1–3):175–207. **doi:10.1016/0025-3227(77)90052-4**

Emerson, S., and Bender, M., 1981. Carbon fluxes at the sediment-water interface of the deep-sea: calcium carbonate preservation. *J. Mar. Res.,* 39:139–162.

Farrell, J.W., Raffi, I., Janecek, T.C., Murray, D.W., Levitan, M., Dadey, K.A., Emeis, K.-C., Lyle, M., Flores, J.-A., and Hovan, S., 1995. Late Neogene sedimentation patterns in the eastern equatorial Pacific Ocean. *In* Pisias, N.G., Mayer, L.A., Janecek, T.R., Palmer-Julson, A., and van Andel, T.H. (Eds.), *Proc. ODP, Sci. Results,* 138: College Station, TX (Ocean Drilling Program), 717–756.

Gartner, S., 1977. Calcareous nannofossil biostratigraphy and revised zonation of the Pleistocene. *Mar. Micropaleontol.,* 2:1–25. **doi:10.1016/0377-8398(77)90002-0**

Haq, B.U., Hardenbol, J., and Vail, P.R., 1987. Chronology of fluctuating sea levels since the Triassic. *Science,* 235:1156–1167.

Hay, W.W., 1970. Calcareous nannofossils from cores recovered on Leg 4. *In* Bader, R.G., Gerard, R.D., et al., *Init. Repts. DSDP,* 4: Washington (U.S. Govt. Printing Office), 455–501.

Kemp, A.E.S., 1995. Neogene and Quaternary pelagic sediments and depositional history of the eastern equatorial Pacific Ocean (Leg 138). *In* Pisias, N.G., Mayer, L.A., Janecek, T.R., Palmer-Julson, A., and van Andel, T.H. (Eds.), *Proc. ODP, Sci. Results,* 138: College Station, TX (Ocean Drilling Program), 627–639.

Kemp, A.E.S., and Baldauf, J.G., 1993. Vast Neogene laminated diatom mat deposits from the eastern equatorial Pacific Ocean. *Nature (London, U. K.),* 362:141–144. **doi:10.1038/362141a0**

Kemp, A.E.S., Baldauf, J.G., and Pearce, R.B., 1995. Origins and paleoceanographic significance of laminated diatom ooze from the eastern equatorial Pacific Ocean. *In* Pisias, N.G., Mayer, L.A., Janecek, T.R., Palmer-Julson, A., and van Andel, T.H. (Eds.), *Proc. ODP, Sci. Results,* 138: College Station, TX (Ocean Drilling Program), 641–645.

King, T.A., Ellis, W.G., Jr., Murray, D.W., Shackleton, N.J., and Harris, S., 1997. Miocene evolution of carbonate sedimentation at the Ceara Rise: a multivariate date/proxy approach. *In* Shackleton, N.J., Curry, W.B., Richter, C., and Bralower, T.J. (Eds.), *Proc. ODP, Sci. Results,* 154: College Station, TX (Ocean Drilling Program), 349–365. **doi:10.2973/odp.proc.sr.154.116.1997**

Knüttel, S., 1986. Calcareous nannofossil biostratigraphy of the central East Pacific Rise, Deep Sea Drilling Project Leg 92: evidence for downslope transport of sediments. *In* Leinen, M., Rea, D.K., et al., *Init. Repts. DSDP,* 92: Washington (U.S. Govt. Printing Office), 255–290.

Lyle, M., Dadey, K.A., and Farrell, J.W., 1995. The late Miocene (11–8 Ma) eastern Pacific carbonate crash: evidence for reorganization of deep-water circulation by the closure of the Panama Gateway. *In* Pisias, N.G., Mayer, L.A., Janecek, T.R., Palmer-Julson, A., and van Andel, T.H. (Eds.), *Proc. ODP, Sci. Results,* 138: College Station, TX (Ocean Drilling Program), 821–838.

Martini, E., 1971. Standard Tertiary and Quaternary calcareous nannoplankton zonation. *In* Farinacci, A. (Ed.), *Proc. 2nd Int. Conf. Planktonic Microfossils Roma:* Rome (Ed. Tecnosci.), 2:739–785.

Martini, E., and Müller, C., 1986. Current Tertiary and Quaternary calcareous nannoplankton stratigraphy and correlations. *Newsl. Stratigr.,* 16:99–112.

Mayer, L.A., Shipley, T.H., and Winterer, E.L., 1986. Equatorial Pacific seismic reflectors as indicators of global oceanographic events. *Science,* 233:761–764.

Okada, H., and Bukry, D., 1980. Supplementary modification and introduction of code numbers to the low-latitude coccolith biostratigraphic zonation (Bukry, 1973; 1975). *Mar. Micropaleontol.,* 5:321–325. **doi:10.1016/0377-8398(80)90016-X**

Paytan, A., Kastner, M., and Chavez, F.P., 1996. Glacial to interglacial fluctuations in productivity in the equatorial Pacific as indicated by marine barite. *Science,* 274:1355–1357. **doi:10.1126/science.274.5291.1355**

Perch-Nielsen, K., 1985. Cenozoic calcareous nannofossils. *In* Bolli, H.M., Saunders, J.B., and Perch-Nielsen, K. (Eds.), *Plankton Stratigraphy:* Cambridge (Cambridge Univ. Press), 427–554.

Peterson, L.C., Murray, D.W., Ehrmann, W.U., and Hempel, P., 1992. Cenozoic carbonate accumulation and compensation depth changes in the Indian Ocean. *In* Duncan, R.A., Rea, D.K., Kidd, R.B., von Rad, U., and Weissel, J.K. (Eds.), *Synthesis of Results from Scientific Drilling in the Indian Ocean*. Geophys. Monogr., 70:311–333.

Pisias, N.G., Mayer, L.A., and Mix, A.C., 1995. Paleoceanography of the eastern equatorial Pacific during the Neogene: synthesis of Leg 138 drilling results. *In* Pisias, N.G., Mayer, L.A., Janecek, T.R., Palmer-Julson, A., and van Andel, T.H. (Eds.), *Proc. ODP, Sci. Results,* 138: College Station, TX (Ocean Drilling Program), 5–21.

Raffi, I., Backman, J., Rio, D., and Shackleton, N.J., 1993. Plio–Pleistocene nannofossil biostratigraphy and calibration to oxygen isotopes stratigraphies from Deep Sea Drilling Project Site 607 and Ocean Drilling Program Site 677. *Paleoceanography,* 8:387–408.

Raffi, I., and Flores, J.-A., 1995. Pleistocene through Miocene calcareous nannofossils from eastern equatorial Pacific Ocean. *In* Pisias, N.G., Mayer, L.A., Janecek, T.R., Palmer-Julson, A., and van Andel, T.H. (Eds.), *Proc. ODP, Sci. Results,* 138: College Station, TX (Ocean Drilling Program), 233–286.

Raffi, I., Rio, D., d'Atri, A., Fornaciari, E., and Rocchetti, S., 1995. Quantitative distribution patterns and biomagnetostratigraphy of middle and late Miocene calcare-

ous nannofossils from equatorial Indian and Pacific Oceans (Leg 115, 130, and 138). *In* Pisias, N.G., Mayer, L.A., Janecek, T.R., Palmer-Julson, A., and van Andel, T.H. (Eds.), *Proc. ODP, Sci. Results,* 138: College Station, TX (Ocean Drilling Program), 479–502.

Rea, D.K., and Janecek, T.R., 1986. Grain size changes in reworked pelagic sediments, Deep Sea Drilling Project Site 599. *In* Leinen, M., Rea, D.K., et al., *Init. Repts. DSDP,* 92: Washington (U.S. Govt. Printing Office), 341–343.

Roth, J.M., Droxler, A.W., and Kameo, K., 2000. The Caribbean carbonate crash at the middle to late Miocene transition: linkage to the establishment of the modern global ocean conveyor. *In* Leckie, R.M., Sigurdsson, H., Acton, G.D., and Draper, G. (Eds.), *Proc. ODP, Sci. Results,* 165: College Station, TX (Ocean Drilling Program), 249–273. **doi:10.2973/odp.proc.sr.165.013.2000**

Shackleton, N.J., Baldauf, J.G., Flores, J.-A., Iwai, M., Moore, T.C., Jr., Raffi, I., and Vincent, E., 1995. Biostratigraphic summary for Leg 138. *In* Pisias, N.G., Mayer, L.A., Janecek, T.R., Palmer-Julson, A., and van Andel, T.H. (Eds.), *Proc. ODP, Sci. Results,* 138: College Station, TX (Ocean Drilling Program), 517–536.

Shipboard Scientific Party, 2003. Leg 206 Preliminary Report. *ODP Prelim. Rpt.,* 106 [Online]. Available from World Wide Web: <**http://www-odp.tamu.edu/publications/prelim/206_prel/206PREL.PDF**>. [Cited 2003-02-03]

van Andel, T.H., Heath, G.R., and Moore, T.C., Jr., 1975. Cenozoic history of the central equatorial Pacific Ocean: a synthesis based on Deep Sea Drilling Project data. In *The Geophysics of the Pacific Ocean Basin and its Margin*. Geophys. Monogr., 19:281–296.

Wei, W., 1995. Calibrations of upper Miocene–Pliocene nannofossil datums with magnetostratigraphy, ODP Site 758 in the equatorial Indian Ocean. *In* Flores, J.-A., and Sierro, F.J. (Eds.), *Proc. 5th INA Conf., Salamanca 1993:* Salamanca (Univ. Salamanca Press), 289–299.

Wilson, D.S., 1996. Fastest known spreading on the Miocene Cocos–Pacific plate boundary. *Geophys. Res. Lett.,* 23:3003–3006. **doi:10.1029/96GL02893**

Wise, S.W., 1977. Chalk formation: early diagenesis. *In* Anderson, N.R., and Malahoff, A. (Eds.), *The Fate of Fossil Fuel CO_2 in the Oceans:* New York (Plenum Press), 717–739.

Wise, S.W., Covington, J.M., Ladner, B.C., and Wei, W. (Eds.), 2004. Electronic calcareous nannofossils (version 3). *Int. Nannoplankton Assoc., CD-ROM Ser.,* 1.

Woodruff, F., and Savin, S.M., 1989. Miocene deepwater oceanography. *Paleoceanography,* 4:87–140.

APPENDIX

Species List

Calcareous nannofossils considered in this paper in alphabetical order of generic epithets.

Amaurolithus amplificus (Bukry and Percival, 1971) Gartner and Bukry, 1975
Amaurolithus primus (Bukry and Percival, 1971) Gartner and Bukry, 1975
Amaurolithus ninae Perch-Nielsen, 1977
Amaurolithus tricorniculatus (Gartner, 1967) Gartner and Bukry, 1975
Calcidiscus macintyrei (Bukry and Bramlette, 1969) Loeblich and Tappan, 1978
Calcidiscus premacintyrei Theodoridis, 1984
Catinaster coalitus Martini and Bramlette, 1963
Catinaster mexicanus Bukry, 1971
Ceratolithus acutus Gartner and Bukry, 1974
Ceratolithus armatus Müller, 1974
Ceratolithus cristatus Kamptner, 1950, emend. Bukry and Bramlette 1968
Ceratolithus rugosus Bukry and Bramlette, 1968
Ceratolithus telesmus Norris, 1965
Coccolithus miopelagicus Bukry, 1971, emend. Wise, 1973
Coccolithus pelagicus (Wallich, 1877) Schiller, 1930
Coronocyclus nitescens (Kamptner, 1963) Bramlette and Wilcoxon, 1967
Cyclicargolithus abisectus (Müller, 1970) Wise, 1973
Cyclicargolithus floridanus (Hay et al., 1967) Bukry, 1971
Discoaster adamanteus Bramlette and Wilcoxon, 1967
Discoaster asymmetricus Gartner, 1969
Discoaster aulakos Gartner, 1967
Discoaster bellus Bukry and Percival, 1971
Discoaster berggrenii Bukry, 1971
Discoaster blackstockae Bukry, 1973
Discoaster bollii Martini and Bramlette, 1963
Discoaster braarudii Bukry, 1971
Discoaster brouweri Tan Sin Hok, 1927, emend. Bramlette and Riedel, 1954
Discoaster calcaris Gartner, 1967
Discoaster challengeri Bramlette and Riedel, 1954
Discoaster decorus (Bukry, 1971) Bukry, 1973
Discoaster deflandrei Bramlette and Riedel, 1954
Discoaster exilis Martini and Bramlette, 1963
Discoaster hamatus Martini and Bramlette, 1963
Discoaster icarus Stradner, 1973
Discoaster intercalaris Bukry, 1971
Discoaster kugleri Martini and Bramlette, 1963
Discoaster loeblichii Bukry, 1971
Discoaster mendomobensis Wise, 1973
Discoaster micros (Theodoridis, 1984) Kaenel and Villa, 1996
Discoaster moorei Bukry, 1971
Discoaster neohamatus Bukry and Bramlette, 1969
Discoaster neorectus Bukry, 1971

Discoaster pansus (Bukry and Percival, 1971) Bukry, 1973
Discoaster pentaradiatus Tan Sin Hok, 1927, emend. Bramlette and Riedel, 1954
Discoaster perclarus Hay in Hay et al., 1967
Discoaster prepentaradiatus Bukry and Percival, 1971
Discoaster pseudovariabilis Martini and Worsley, 1971
Discoaster quinqueramus Gartner, 1969
Discoaster sanmiguelensis Bukry, 1981
Discoaster surculus Martini and Bramlette, 1963
Discoaster tristellifer Bukry, 1976
Discoaster variabilis Martini and Bramlette, 1963
Emiliania huxleyi (Lohmann, 1902) Hay and Mohler in Hay et al., 1967
Gephyrocapsa caribbeanica Boudreaux and Hay, 1967
Gephyrocapsa oceanica Kamptner, 1943
Gephyrocapsa Kamptner, 1943 (small)
Hayaster perplexus (Bramlette and Riedel, 1954) Bukry, 1973
Helicosphaera burkei Black, 1971
Helicosphaera carteri (Wallich, 1877) Kamptner, 1954
Helicosphaera euphratis Haq, 1966
Helicosphaera granulata (Bukry and Percival, 1971) Jafar and Martini, 1975
Helicosphaera inversa Gartner, 1980
Helicosphaera kamptneri (Hay and Mohler in Hay et al., 1967) Locker, 1973
Helicosphaera sellii (Bukry and Bramlette, 1969) Jafar and Martini, 1975
Helicosphaera walbersdorfensis Müller, 1974
Helicosphaera wallichii (Lohmann, 1902) Boudreaux and Hay, 1969
Pontosphaera japonica (Takayama, 1967) Nishida, 1971
Pontosphaera multipora (Kamptner, 1948) Roth, 1970, emend. Burns, 1973
Pontosphaera versa (Bramlette and Sullivan, 1961) Sherwood, 1974
Pseudoemiliania lacunosa (Kamptner, 1963) Gartner, 1969
Reticulofenestra gelida (Geitzenauer, 1972) Backman, 1978
Reticulofenestra haqii Backman, 1978
Reticulofenestra [= *Dictyococcites*] *minuta* Roth, 1970
Reticulofenestra minutula (Gartner, 1967) Haq and Berggren, 1978
Reticulofenestra perplexa (Burns, 1975) Wise, 1983
Reticulofenestra producta (Kamptner, 1963) Wei and Thierstein, 1991
Reticulofenestra pseudoumbilica (Gartner, 1967) Gartner, 1969
Reticulofenestra rotaria Theodoridis, 1984
Rhabdosphaera clavigera Murray and Blackman, 1898
Rhabdosphaera procera Martini, 1969, emend. Jafar, 1975
Scapholithus fossilis Deflandre in Deflandre and Fert, 1954
Scyphosphaera Lohmann, 1902
Sphenolithus abies Deflandre in Deflandre and Fert, 1954
Sphenolithus compactus Backman, 1980
Sphenolithus heteromorphus Deflandre, 1953
Sphenolithus moriformis (Brönnimann and Stradner, 1960) Bramlette and Wilcoxon, 1967
Sphenolithus neoabies Bukry and Bramlette, 1969
Sphenolithus verensis Backman, 1978
Syracosphaera pulchra Lohmann, 1902

Triquetrorhabdulus rugosus Bramlette and Wilcoxon, 1967
Umbellosphaera irregularis Paasche in Markali and Paasche, 1955
Umbilicosphaera jafari Müller, 1974
Umbilicosphaera rotula (Kamptner, 1956) Varol, 1982
Umbilicosphaera sibogae (Weber-van Bosse, 1901) Gaarder, 1971

Figure F1. Backtracked path for Leg 206 Site 1256 and locations of Leg 138 sites. The backtracking is shown at 1-m.y. increments, with the last point in the path indicating the location of the site when the basement formed (after Shipboard Scientific Party, 2003; Pisias et al., 1995).

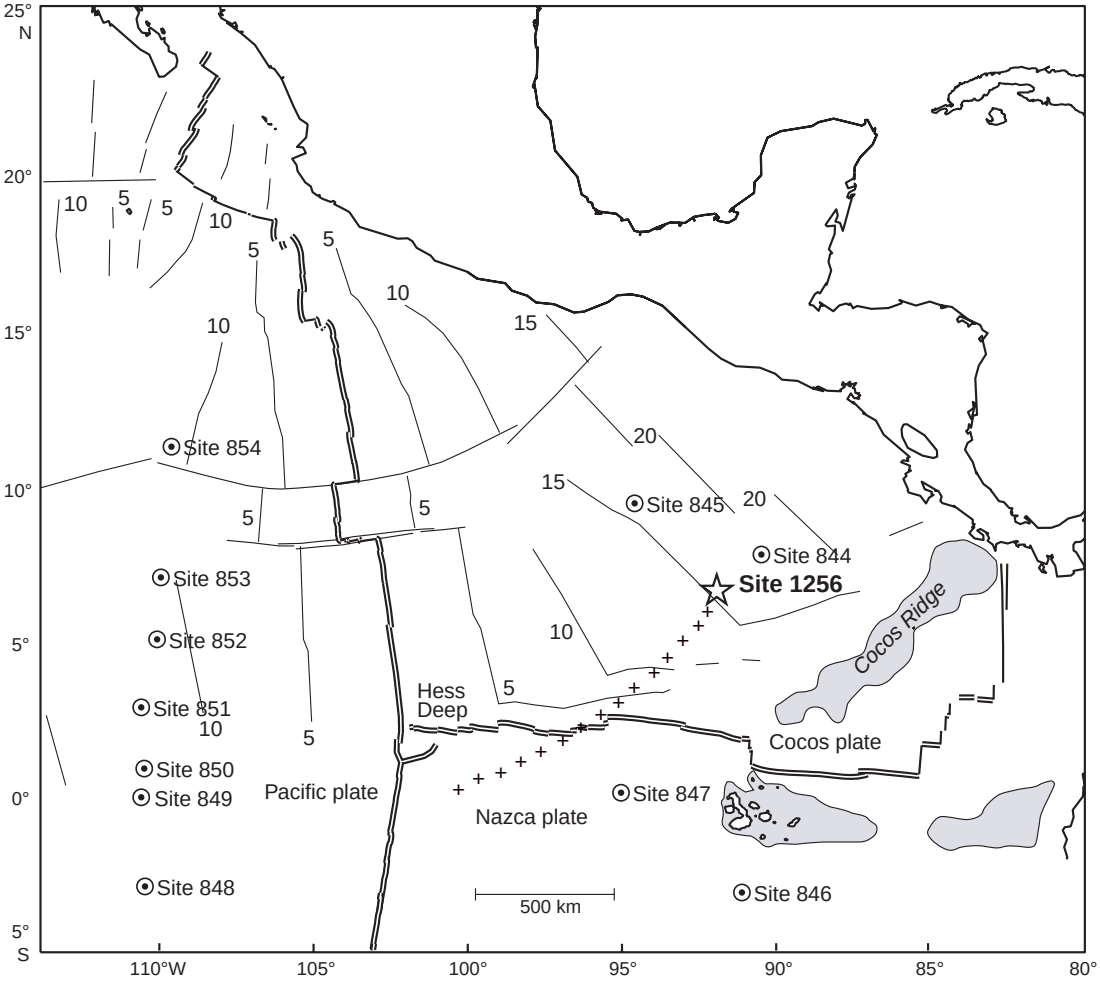

Figure F2. A. Linear sedimentation rates as constrained by the biostratigraphy and magnetostratigraphy, and a best-fit linear sedimentation rate model. The linear rates are shown extrapolated to basement. Nannofossil datum age estimates and depths are presented in Table T2, p. 24. FO = first occurrence, LO = last occurrence. Magnetostratigraphy data are from Shipboard Scientific Party (2003). **B.** Calcareous nannofossil datum age-depth plots for eastern equatorial Pacific drill holes. Data for Sites 844–853 are from Raffi and Flores (1995).

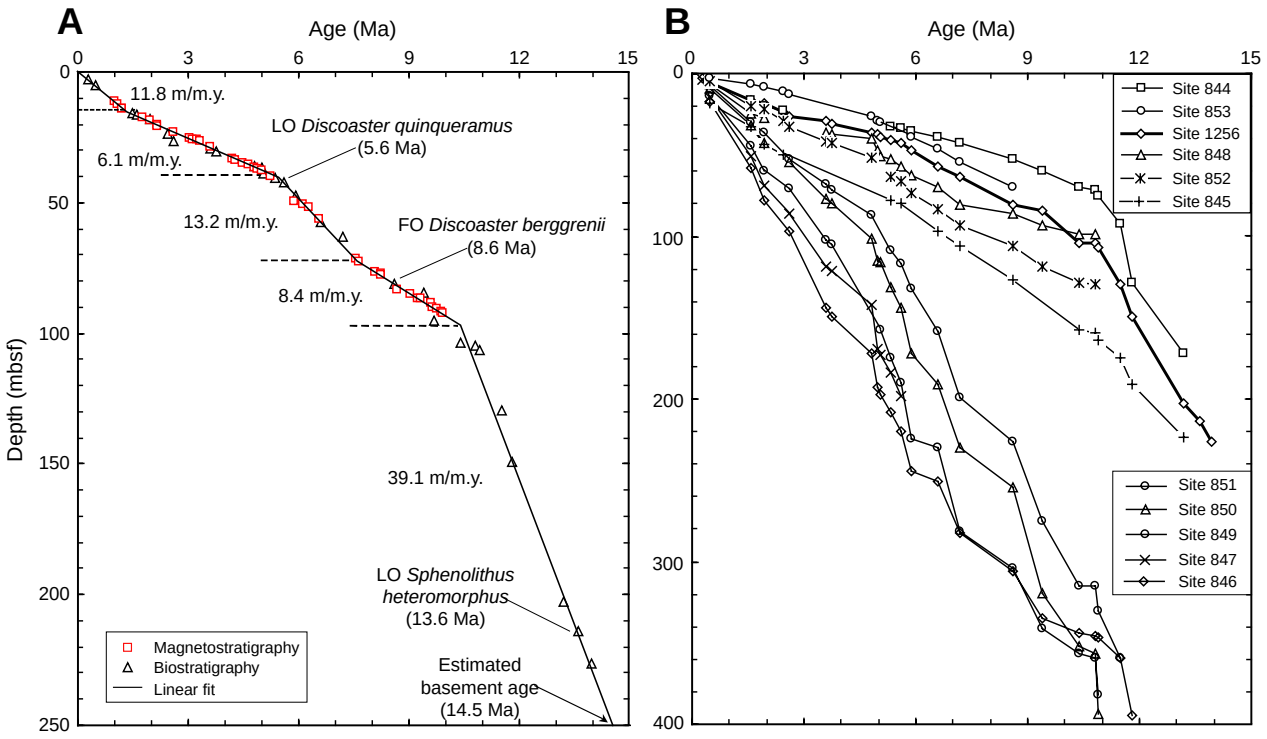

Figure F3. Relationship of mass accumulation rates between bulk sediments and the main sedimentary components. Note the change of scale for $CaCO_3$ in the 0- through 9-Ma interval.

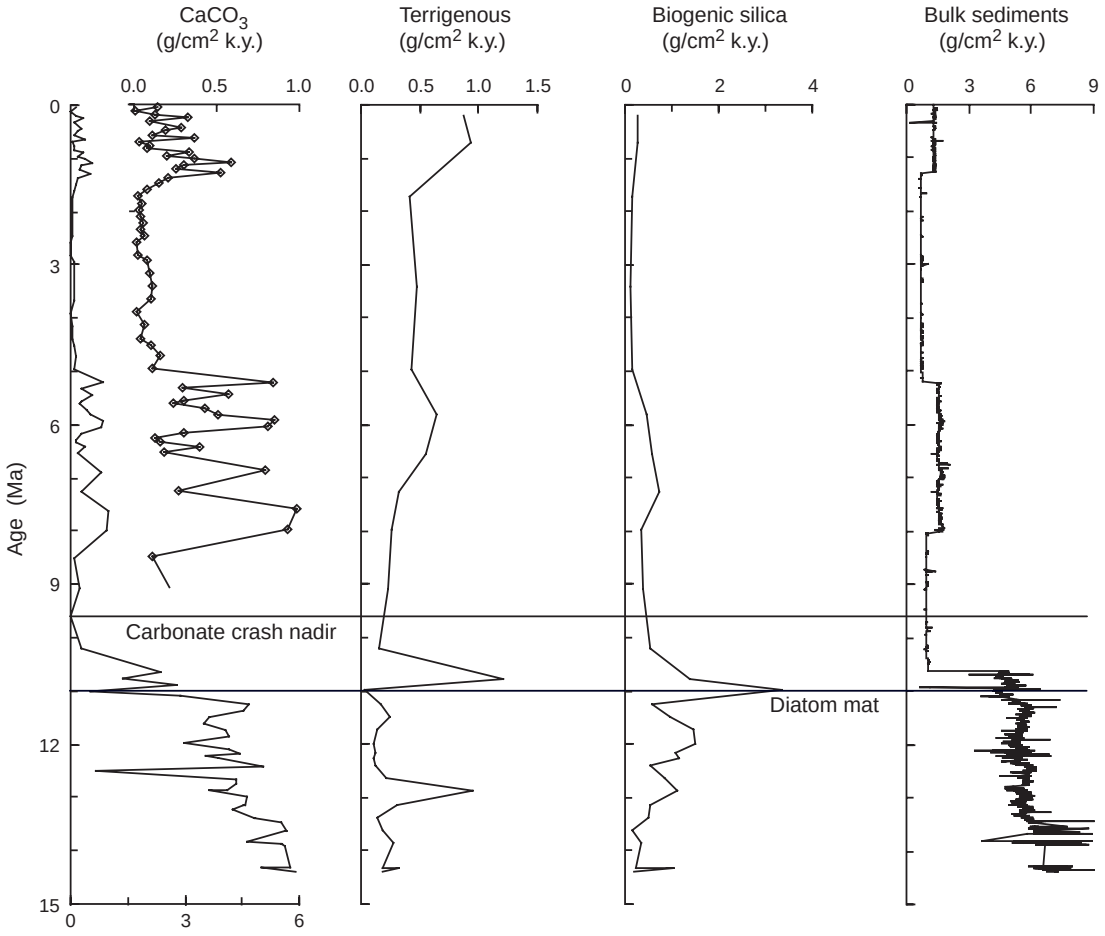

Figure F4. Correlation of nannofossil datums in EEP drill holes that reflects variations in sedimentation rates over time. Data for Sites 844–853 are from Raffi and Flores (1995). Heavy lines approximate epoch boundaries. The numerical age for each correlation line is listed in chronological order in the lower left box.

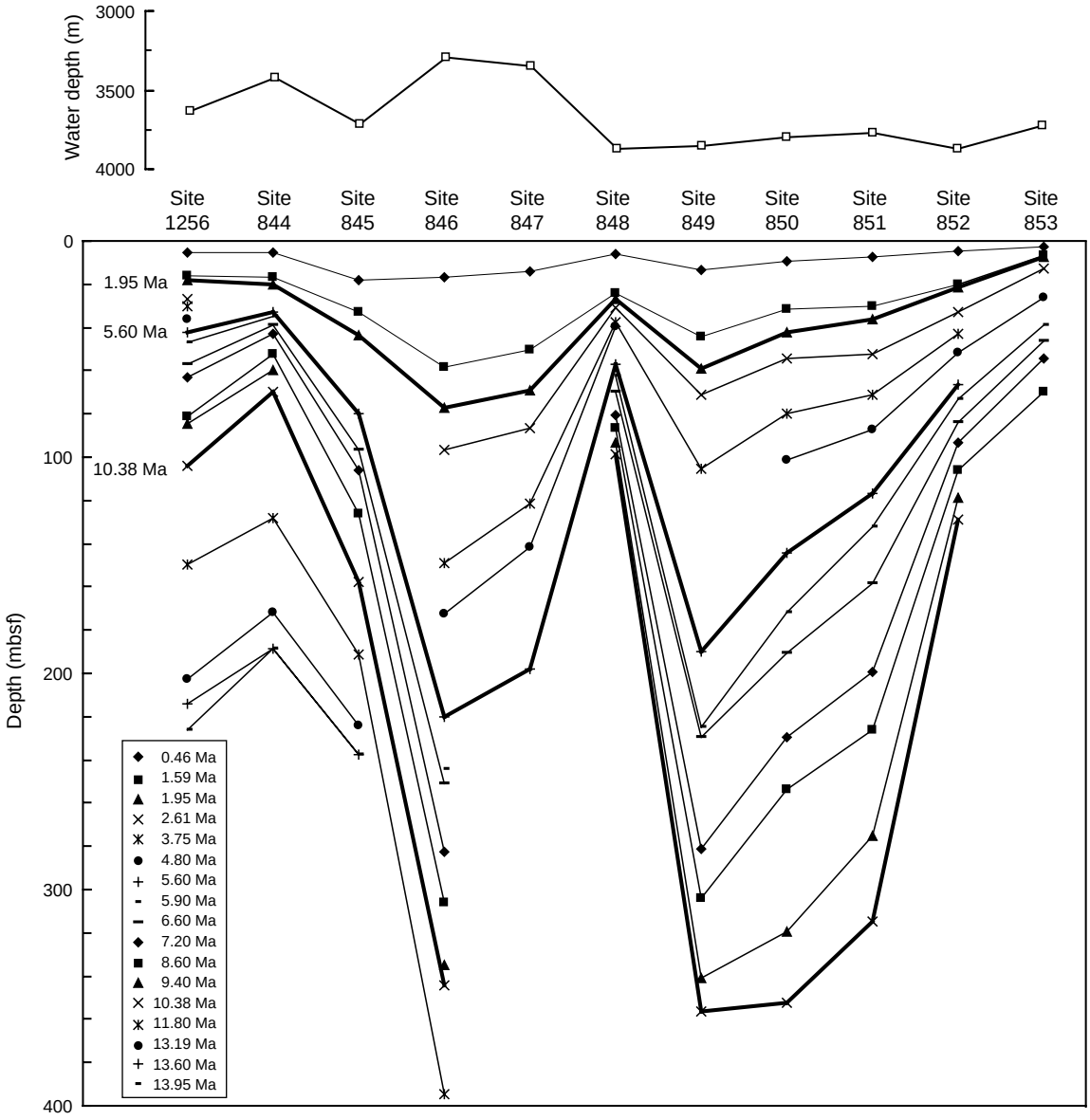

Table T1. Calcareous nannofossil distribution chart in Hole 1256B. (This table is available in an **oversized format.**)

Table T2. Age estimate, depth, and zonation of calcareous nannofossil datum levels used in this study.

Biohorizons	Zone (base)		Core, section, interval (cm)		Depth (mbsf)			Age (Ma)	Reference
	NN	CN	Top	Bottom	Top	Bottom	Mean		
			206-1256B-	206-1256B-					
FO *Emiliania huxleyi*	NN21	CN15	1H-2, 40–42	1H-3, 40–42	1.90	3.40	2.65	0.26	1
LO *Pseudoemiliania lacunosa*	NN20	CN14b	1H-4, 40–42	1H-4, 115–117	4.90	5.65	5.28	0.46	1
LO *Helicosphaera sellii*	NN19b		2H-7, 40–42	2H-CC	15.47	15.91	15.69	1.47	1
LO *Calcidiscus macintyrei*			3H-1, 40–42	3H-1, 115–117	16.00	16.75	16.38	1.59	1
LO *Discoaster brouweri*	NN19a	CN13	3H-1, 115–117	3H-3, 115–117	16.75	19.75	18.25	1.95	1
LO *Discoaster pentaradiatus*	NN18	CN12d	3H-5, 115–117	3H-7, 40–42	22.75	25.00	23.88	2.44	2
LO *Discoaster surculus*	NN17	CN12c	4H-1, 115–117	4H-2, 40–42	26.25	27.00	26.63	2.61	2
LO *Sphenolithus abies/neoabies*	NN16		4H-3, 40–42	4H-4, 40–42	28.50	30.00	29.25	3.60	1
LO *Reticulofenestra pseudoumbilica*		CN12a	4H-4, 40–42	4H-4, 115–117	30.00	30.75	30.38	3.75	1
LO *Amaurolithus* spp. (*A. primus*)		CN11a	5H-1, 115–117	5H-2, 40-42	35.75	36.50	36.13	4.80	1
LO *Ceratolithus acutus*		CN10c	5H-2, 40–42	5H-2, 115–117	36.50	37.25	36.88	4.99	3
FO *Ceratolithus rugosus*	NN13		5H-3, 115–117	5H-4, 40-42	38.75	39.50	39.13	5.04	2
FO *Ceratolithus acutus*	NN12	CN10b	5H-4, 115–117	5H-5, 40–42	40.25	41.00	40.63	5.34	1
LO *Discoaster quinqueramus*		CN10a	5H-5, 115–117	5H-6, 40-42	41.75	42.50	42.13	5.60	4
LO *Amaurolithus amplificus*	NN11d	CN9b	6H-2, 115-117	6H-3, 40–42	46.75	47.50	47.13	5.90	4
FO *Amaurolithus amplificus*	NN11c		7H-3, 40–42	7H-3, 115–117	57.00	57.75	57.38	6.60	4
FO *Amaurolithus primus*	NN11b		7H-7, 40–42	7H-CC	63.00	63.39	63.20	7.20	4
FO *Discoaster berggrenii*	NN11a	CN9a	9H-6, 40-42	9H-6, 115–117	80.50	81.25	80.88	8.60	4
LO *Discoaster hamatus*	NN10	CN8	10H-2, 40–42	10H-2, 115–117	84.00	84.75	84.38	9.40	4
LO *Catinaster coalitus*	NN9	CN7	11H-3, 40-42	11H-3, 115-117	95.00	95.75	95.38	9.69	5
FO *Discoaster hamatus*			12H-2, 115–117	12H-2, 115–117	103.75	103.75	103.75	10.38	3
LO *Coccolithus miopelagicus*	NN8	CN6	12H-3, 40-42	12H-3, 40-42	104.50	104.50	104.50	10.80	4
FO *Catinaster coalitus*			12H-4, 40–42	12H-4, 115–117	106.00	106.75	106.38	10.90	4
LO *Discoaster kugleri*	NN7	CN5b	14H-7, 40-42	14-CC	129.50	130.05	129.78	11.50	4
FO *Discoaster kugleri*			17H-1, 40–42	17H-1, 115–117	149.00	149.75	149.38	11.80	4
LCO *Cyclicargolithus floridanus*	NN6	CN5a	23X-6, 115–117	23X-CC	202.35	202.77	202.56	13.19	2
LO *Sphenolithus heteromorphus*			25X-1, 40–42	25X-1, 115–117	213.40	214.15	213.78	13.60	4
FO *Reticulofenestra pseudoumbilica*			26X-3, 40–42	26X-CC	226.10	226.71	226.41	13.95	3

Notes: FO = first occurrence, LO = last occurrence, LCO = last continuous occurrence. The NN zonation codes are after Martini (1971) and Martini and Müller (1986). The CN zonation codes are after Okada and Bukry (1980). 1 = Berggren et al. (1995a), 2 = Raffi and Flores (1995), 3 = Shackleton et al. (1995), 4 = Berggren et al. (1995b), 5 = Backman and Raffi (1997).